Hydrogen activation on Anatase TiO2: Effect of surface termination

Baohuan Wei, Monica Calatayud

Hydrogen activation on Anatase TiO_2: Effect of Surface Termination

Baohuan Wei[a], Monica Calatayud[a,*]

[a]*Sorbonne Université, CNRS, Laboratoire de Chimie Théorique, 4 Place Jussieu, Paris, France*

Abstract

The mechanisms of H_2 dissociation on three stoichiometric anatase TiO_2 terminations, (001), (100) and (101), have been studied by means of density functional theory (PBE+U) calculations. A two-step process was considered: first, H_2 dissociation into H^+ and H^- pair, and second the H^- species migrates to a neighboring O site, transferring the electrons to the substrate. On (001), it shows the lowest activation barriers for hydrogen dissociation, 0.37 eV, whereas the highest value was found on (101), 0.98 eV. For hydrogen transfer from Ti to near O, the activation barriers are higher (from 1.10 to 2.37 eV), which indicates the dissociation step is kinetically more favorable than the H transfer process, although the latter is thermodynamically more favorable. Electronic structure, vibrational frequency analysis as well as temperature effects are studied to characterize the reactivity. The relationship between electronic structure, geometry and reactivity is analyzed by means of reactivity descriptors, and the results are compared with ceria and rutile TiO_2 facets.

Keywords: Titanium, Hydrogen dissociation, H_2

1. Introduction

Titanium dioxide (TiO_2) is a technologically important material with a wide variety of applications in fields like photocatalysis [1, 2],solar cells [3], catalysis [4, 5], gas sensors[6, 7], lithium-ion batteries [8], or photovoltaic cells [9, 10]. Rutile and anatase are typical polymorphs of TiO_2. While rutile is

*Corresponding Author

Email address: calatayu@lct.jussieu.fr (Monica Calatayud)

the most stable form for larger particles, most nanomaterials are in anatase phase due to the relatively lower surface energy of (101) and (100) [11, 12]. Of the anatase phase, (101) is the most stable and frequently exposed surface [13, 14, 15, 16]. The (101) and (100) are found in solar cell devices [17, 18], and the (001) and (100) are present in the P25 catalyst [19]. Although the (001) is only a minority surface, experimental and theoretical studies indicate that the anatase (001) surface is very reactive due to the low-coordination of its surface atoms [20, 21, 22, 23, 24].

The presence of hydrogen in titania is not surprising. Frequently, adsorbed hydrogen is commonly observed on TiO_2 surfaces due to the standard surface science cleaning procedures [25], or is achieved by direct adsorption of atomic atoms on single crystals[26]. Moreover, hydrogenated TiO_2 is found to exhibit high photocatalytic activity [27, 28]. Hydrogen is found as a proton in surface hydroxyl groups. However, recent works on another reducible oxide, ceria, show that hydride intermediates could play a major role in the dissociation of H_2 on the surface [29, 30, 31]. The stability of such hydride species has been found for rutile surfaces [32, 33]. In this work we aim at understanding the behavior of hydrogen on stoichiometric TiO_2 anatase surfaces, paying special attention to the role of surface topology.

For TiO_2, it has been well established that the product of hydrogenation leads to stable hydroxylated species [24, 26, 34, 35, 36]. Titanium hydride intermediate was studied theoretically[32, 33] and experimentally observed[37]. Based on these works, a two-step mechanism of hydrogen dissociation on TiO_2 was proposed: H_2 dissociates on the bare surface through a heterolytic pathway (forming a hydride/proton pair), followed by H atom transferring from Ti atom to nearby O, that finally yields the homolytic product (forming two hydroxyl groups and reducing two Ti atoms).

Hydrogen dissociation on TiO_2 has attracted attention by recent theoretical research studies [24, 32, 33]. Hu et al. studied H_2 dissociation on three TiO_2 polymorphs [33], which indicated that homolytic activation barriers are high (1.48–1.68 eV), and the rutile phase showed the highest activity. Recently, we reported the H_2 activation on four rutile TiO_2 terminations, indicating that the heterolytic dissociation pathway is kinetically more favorable than the H transfer process, although the product with only surface hydroxyl groups, is thermodynamically more favorable. Irregular surfaces of gas-phase clusters are also able to dissociate hydrogen [36, 38]. Although the computational results indicated that hydride surfaces on TiO_2 surfaces are metastable, few Ti-H hydride is observed experimentally. The conflicting

reports of hydride on TiO_2 surfaces motivated us to address the role of the hydride species during the dissociation process.

To the best of our knowledge, the orientation effect of anatase phase TiO_2 for H_2 dissociation has not been addressed in the literature, and is the primary focus of the present work. In the present work we analyze three relevant anatase TiO_2 surfaces: (001), (100), and (101), and their role in the H_2 dissociation two-step process. Periodic PBE+U calculations were used to obtain the energetics of the process. Vibrational frequencies for TiH and OH are also reported as a guide to identify relevant species on the different facets. Electronic structure analysis is carried out to fully characterize the nature of the relevant structures. Finally, and based on our previous studies, the comparison with the rutile phase and ceria is carried out.

2. Computational Method and Materials

2.1. Methods

We performed density functional theory (DFT) calculations using the Vienna ab initio simulation package (VASP) version 5.4.4 [39]. Core electrons are represented by the projector-augmented wave (PAW) pseudopotentials with 1, 4, and 6 valence electrons for H, Ti, and O, respectively [40]. The generalized gradient approximation (GGA) approach was applied for the exchange and correlation potential with the Perdew–Burke–Erzenhof (PBE) functional [41], spin-polarized. The GGA+U approach of Dudarev et al. was used to treat the 3d orbital electrons of Ti with the effective Hubbard on-site Coulomb interaction parameter ($U' = U - J$) [42]. We chose $U' = 4$ according to the proposed value from previous works [34, 43]. A 400 eV cutoff energy for the plane-wave basis set was found to correctly treat the valence electrons. The energies were converged to 10^{-4} eV for the electronic loop, and the forces acting on each atom were less than 0.03 eV/Å. The Brillouin zone was sampled with the Monkhorst Pack k-point mesh with the kpoints spaced 0.05 $Å^{-1}$ in the reciprocal space. The dispersion was not included because in our previous work of H reaction with rutile surfaces, the effects were considered negligible [32].

Transition states were located by a two step processes. First, the Climbing Image Nudged Elastic Band(CI-NEB) [44, 45] was used to get a good guess, which includes four images along the reaction coordination and get converged with loose criteria. Then the Improved Dimer Method(IDIM) was applied to find the stationary point [46, 47]. All the transition states were identified

by performing the frequency analysis. Only one imaginary frequency was obtained and was checked to connect to the initial and final states.

The zero point energy(ZPE) was computed as one-half of the sum of real vibration frequencies[48]. The Gibbs free energy at room temperature (298K) was also considered :

$$G(T) = H - TS = U + pV - TS \approx U(T) - TS(T) \tag{1}$$

For the adsorption system, it is reasonable to consider only the vibrational contributions:

$$U(T) = E_{DFT} + E_{ZPE} + U_{vib}(T) \tag{2}$$

$$S(T) = S_{vib}(T) \tag{3}$$

$$U_{vib}(T) = \sum_{i=1}^{3N-6} (\frac{h\nu_i}{e^{-\frac{h\nu_i}{K_B T}} - 1}) \tag{4}$$

$$S_{vib}(T) = K_B \sum_{i=1}^{3N-6} (\frac{h\nu_i}{K_B T(e^{-\frac{h\nu_i}{K_B T}} - 1)}) - ln(1 - e^{-\frac{h\nu_i}{K_B T}}) \tag{5}$$

Thus,

$$G(T) \approx F(T) = E_{DFT} + E_{ZPE} + K_B T \sum_{i=1}^{3N-6} [ln(1 - e^{-\frac{h\nu_i}{K_B T}})] \tag{6}$$

The density-functional perturbation theory (DFPT) linear response approach was employed to obtain vibrational spectra and intensity[49]. Firstly, the matrix of Born effective charges (BEC), which indicates the polarizabilities' change of involved atoms, is calculated. The infrared intensity is computed based on the following formula:

$$I_{\omega}^{IR} \propto \sum_{\alpha=1}^{3} | \sum_{i=1}^{M} \sum_{\beta=1}^{3} Z_{\alpha\beta}^{\star}(i) e_{\beta}(i)$$

(7)

Where α and β correspond to Cartesian polarization, $Z_{\alpha\beta}^{\star}$ is the effective charge tensor. $e_{\beta}(i)$ indicates normalized vibrational eigenvector.

2.2. Models

The slab models were cut from the optimized structure of bulk anatase (a = b = 3.870 Å and c = 9.563 Å, close to the experimental values [50] (a = b = 3.782 Å, c= 9.502 Å). A vacuum layer of 15 Å was employed to prevent interaction between slabs. The lower-half layers of the slab were kept frozen and the upper-half layers were allowed to relax.

The adsorption of hydrogen on TiO_2 surfaces was investigated in the 2*2 unit cell for (001) and 1*2 for (100) and (101). The slabs used can be found in the supplementary information. The size, composition, coordination number of surface sites for three anatase surfaces are shown in Figure 1 and Table 1. Only the stoichiometric terminations are studied; the three facets are roughly flat. On (001) and (100), there only exists five-fold Ti_{5C} coordinated titanium sites, while (101) has Ti_{5C} and Ti_{6C}. Regarding oxygen, (001) has only surface O_{2C}, while the other two exhibit O_{2C} and O_{3C}.

Table 1: Size, composition, coordination number for three anatase slabs.

Type	(001)	(100)	(101)
Supercell	2*2	1*2	1*2
Composition(TiO_2 units)	24	32	32
Atomic layers(frozen/relaxed)	3/3	4/4	2/2
Coordination number of surface site	Ti(5) O(2)	Ti(5) O(2,3)	Ti(5,6) O(2,3)
Surface Energy(J/m^2)	1.06	0.90	0.81
Parameter	a=7.740	a=7.740	a=10.317
	b=7.740	b=9.563	b=7.740

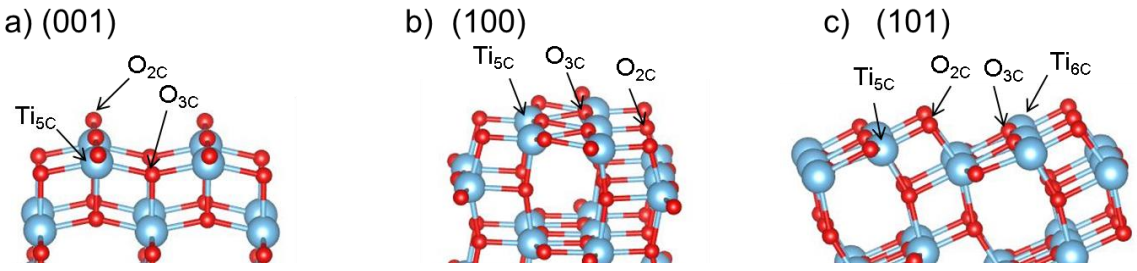

Figure 1: The structures of anatase (001), (100) and (101) surfaces. The Ti atoms are showed by blue balls and the O atoms by red balls.

The adsorption energy E_{ads} on the different substrates was calculated taking as reference the physisorbed H_2* species on the bare slab, according to the equation:

$$E_{ads} = E(\mathrm{TiO_2/H_2}) - E(\mathrm{TiO_2 - H_2*}) \tag{8}$$

The surface energies γ were calculated according to:

$$\gamma = \frac{1}{2A}(E_{slab} - NE_{bulk}) \tag{9}$$

Where E_{slab} is the energy of the bare slab, N is the number of bulk TiO_2 in the slab, E_{bulk} is the bulk energy, and A is the surface area of one side of the slab depending on the terminations considered.

The considered mechanism is shown in Figure 2. Starting from a physisorbed H_2 molecule (H_2* species), the H-H bond breaks through the heterolytic pathway to form a hydride, bonding to the Ti site, and a proton binds to one oxygen to form the (H^+-H^-) species. The transition state involved in this process is labeled as TS1. In a second step, we studied the transfer of the H^- on the Ti site to the nearby O site, resulting in homogeneous dissociation leading to the 2O-H hydroxyl groups, labeled (H^+-H^+). This step is accompanied by a two-electrons transfer to surface titanium sites that become reduced. The transition state associated with this step is labeled as TS2.

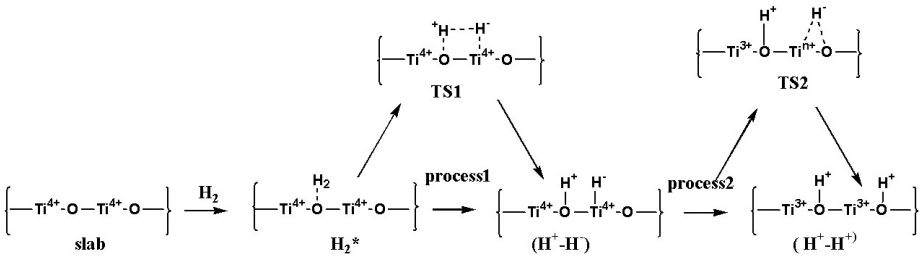

Figure 2: Schematic representations of the different steps considered in the present work. The heterolytic dissociation pathway of H_2 over anatase TiO_2 facet (process 1), followed by sequential H transfer from Ti to near O (process 2). The species are labeled in the scheme.

3. Results and discussion

3.1. Energy and Structure

We firstly investigated the heterolytic pathways for H_2 dissociation, followed by H transfer from Ti to nearby O on these three anatase TiO_2 surfaces. The energetic profile involving different steps is summarized in Table 2 and Figure 3, where all adsorption energies are referenced to the energy of the physisorbed TiO_2-H_2 system. The side views of the paths for the three surfaces are provided in SI (See Figure S1 and Figure S2).

	(001)	(100)	(101)
H_2*	0.00(0.00/0.00)	0.00(0.00/0.00)	0.00(0.00/0.00)
TS1	0.37(0.36/0.36)	0.88(0.91/0.88)	0.98(1.03/1.00)
(H^+-H^-)	-0.10(0.00/0.02)	0.07(0.18/0.16)	0.39(0.50/0.47)
ΔE_1	-0.10(0.00/0.02)	0.07(0.18/0.16)	0.39(0.50/0.47)
ΔE_1^{back}	0.10(0.00/-0.02)	-0.07(-0.18/-0.16)	-0.39(-0.50/-0.47)
E_{act1}^{forw}	0.37(0.36/0.36)	0.88(0.91/0.88)	0.98(1.03/1.00)
E_{act1}^{back}	0.38(0.36/0.34)	0.81(0.73/0.72)	0.59(0.53/0.53)
TS2	1.10(1.15/1.16)	1.98(2.06/2.03)	2.37(2.41/2.37)
E_{act2}^{forw}	1.20(1.15/1.14)	1.92(1.88/1.87)	1.98(1.91/1.90)
(H^+_{O2C}-H^+_{O3C})		-0.23(0.01/-0.01)	
TS3		1.37(1.44/1.42)	
(H^+_{O2C}-H^+_{O2C})	-1.27(-1.03/-1.01)	-1.27(-1.03/-1.04)	-0.77(-0.54/-0.56)
ΔE_2	-1.26(-1.03/-1.03)	-1.34(-1.21/-1.20)	-1.16(-1.04/-1.03)

Table 2: Energy profile for relevant structures, in eV. Inside the parentheses is the energy with ZPE correction as well as at room temperature. All energies are referred to the physisorbed TiO_2-H_2 system.

In the mechanism, the physisorbed species (H_2*), generated by the initial interaction between H_2 and the bare surface, was found to be with slightly elongated H-H bond.

Once physisorbed species (H_2*) is formed, the heterolytic dissociation from H_2* occurs on adjacent Ti and O sites, generating the corresponding Ti-H and O-H bonds. On three terminations, two H atoms preferentially adsorb to atoms with lower coordination numbers O_{2C} and Ti_{5C}, that is ($H^+_{O2C} - H^-_{Ti5C}$), rather than higher coordination numbers Ti_{6C} or O_{3C}. The bond lengths of generated heterolytic products ($H^+_{O2C} - H^-_{Ti5C}$) are around

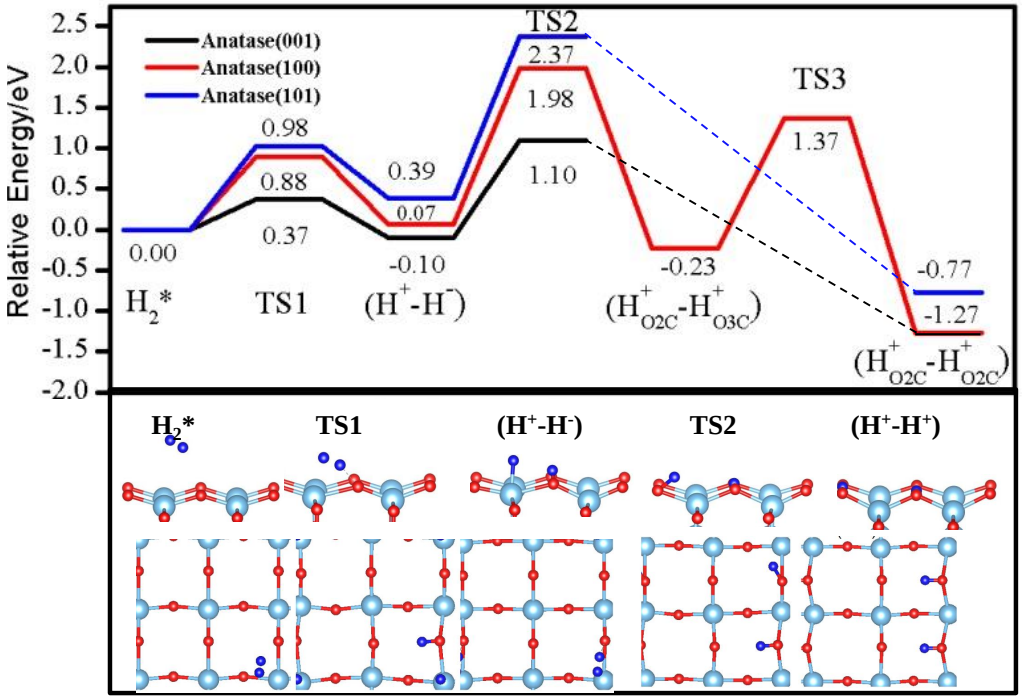

Figure 3: The energy profile of hydrogen dissociation and H transfer from Ti to near O on three anatase TiO_2 surfaces, namely (001), (100) and (101). Images show the pathway (side and top view) for (001). Color code: oxygen atoms in red, Ti in cyan, H in dark blue.

0.980 Å for O-H on the three terminations and Ti-H 1.713 Å on (001), 1.704 Å on (100), 1.699 Å on (101), respectively.

This step is slightly exothermic for the (001) facet (-0.10 eV), while on (100) and (101) terminations, it is endothermic, by 0.07 eV, 0.39 eV respectively. The activation barrier for this step follows the trend (001) 0.37 eV < (100) 0.88 eV < (101) 0.98 eV.

Our results are consistent with previous studies. For the anatase (101) surface, our activation energy barrier (0.98 eV) and reaction energy (0.39 eV) are consistent with the one reported previously[33], 1.04 eV for activation energy and 0.46 eV for reaction energy (See Table S1). The differences are negligible due to slightly difference of calculation details.

For the backward activation (E_{act1}^{back}), it indicates the hydride TiH/OH species recombination to regenerate and desorb H_2 on three terminations,

which require 0.38 eV for (001), 0.81 eV for (100) and 0.59 eV for the (101) slabs. Besides, the desorption of H_2 is slightly endothermic for the (001) terminations (0.01 eV), while it is exothermic for the (110) and (101) by -0.07 eV, by -0.39 eV. Thus, on (001), the dissociation and reversibility recombination of hydrogen occur easily with lower activation barrier (0.37 eV and 0.38 eV, respectively). While on the (100) and (101) terminations, both processes are more difficult to happen due to the higher kinetic energy barriers.

For the process of H transfer from Ti to O, it gives rise to the formation of two OH groups (H^+-H^+). The (H^+, H^+) species are more exothermic, with -1.27 eV on (001) and (100), -0.77 eV on (101). At the same time, it causes the change in the oxidation state of two Ti cations from Ti^{4+} to Ti^{3+}. The activation barriers are significantly higher than the first process: 1.20 eV on (001), 1.92 eV on (100) and 1.98 eV on (101), indicating it is a kinetically unfavorable process from the heterolytic intermediates to the homolytic products.

For the heterolytic dissociation process on (100), the initial distance between the Ti and O sites is too long for a one-step H transfer so it is split in two steps via an intermediate O_{3C} site (barrier of 1.98 eV), followed by the transfer to another 2-fold coordinated oxygen (barrier of 1.37 eV). As for the other terminations, the high barriers would allow the stabilization of the TiH species.

The most thermodynamically stable product for step 2 involves the presence of two hydroxyl groups and two Ti^{3+} sites. The latter originates from the electron transfer from the hydride to two titanium sites. This transfer results in open-shell systems that can be characterized by the presence of two unpaired electrons, as described below.

In conclusion, the heterolytic dissociation process is kinetically more favorable than the H transfer process, although the latter is thermodynamically more favorable.

The structures of the transition states (TS1 and TS2) of the three facets as well as the value of the imaginary frequency are provided in SI (Figure S3, S4 and S5).

3.1.1. Zero Point Energy and Gibbs energy correction

The energy with Zero Point Energy (ZPE) correction and at room temperature are studied to provide more accurate interaction energies. The values are shown in Table 2. In Figure 4 the red line indicates the energy profile with ZPE correction, and the Gibbs energy (T=298 K) is shown with the

blue line for the (001) surface.

With ZPE correction and at room temperature, the thermodynamic energy for these two steps increased slightly, while there is no effect on the activation barriers. The same behavior is observed for the other two surfaces, the details for (100) and (101) are provided in SI (Figure S6 and Figure S7).

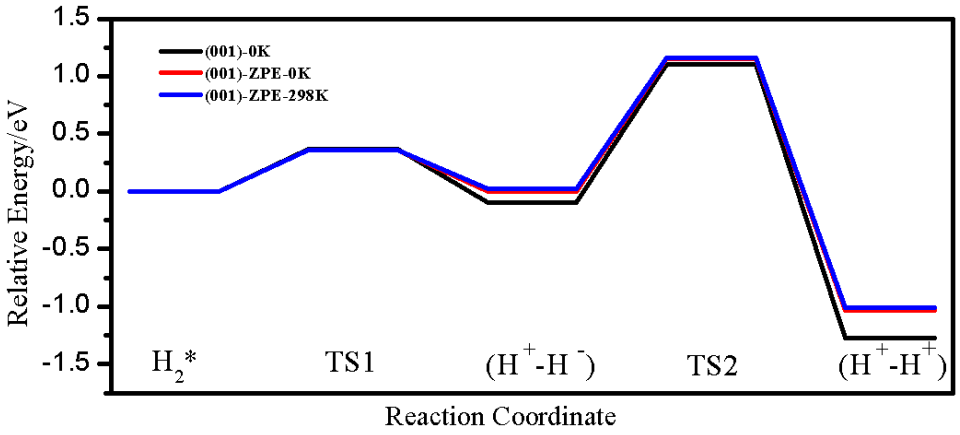

Figure 4: The energetic profile for the two-step dissociation process on anatase(001) surfaces. ZPE zero point energy correction (red lines) and Gibbs free energy T=298 K (blue lines) For (100) and (101) surfaces, it is provided in SI (Figure S6 and Figure S7).

3.2. Electronic Structure

From an electronic point of view, the different steps involved in H_2 dissociation on three anatase facets were clearly identified in the projected density of states (PDOS)(See Figure 5, Figure S8 and Figure S9), where only the projections of related Ti, O and H atoms were depicted for the sake of clarity.

The PDOS is independent of the orientation, and all the surfaces studied show a similar behavior. First, the appearance of a narrow band around 6.0 eV to -4 eV shows the physisadsorption of molecular H_2. For the product of heterolytic dissociation (H^+-H^-), two sharp peaks appear around 6.0 eV associated to proton (H^+) and the Fermi level associated to the hydride species (H^-). Finally, with the formation of the homolytic product (H^+-H^+), the two protons states coming from H_2 molecule are well localized in the narrow band around -6.3 eV. Also, Ti states appear at the Fermi level, indicating the reduction of the Ti sites, which is also consistent with the picture of the spin density of (H^+-H^+) in Figure 6 and Table **??**, which indicates the

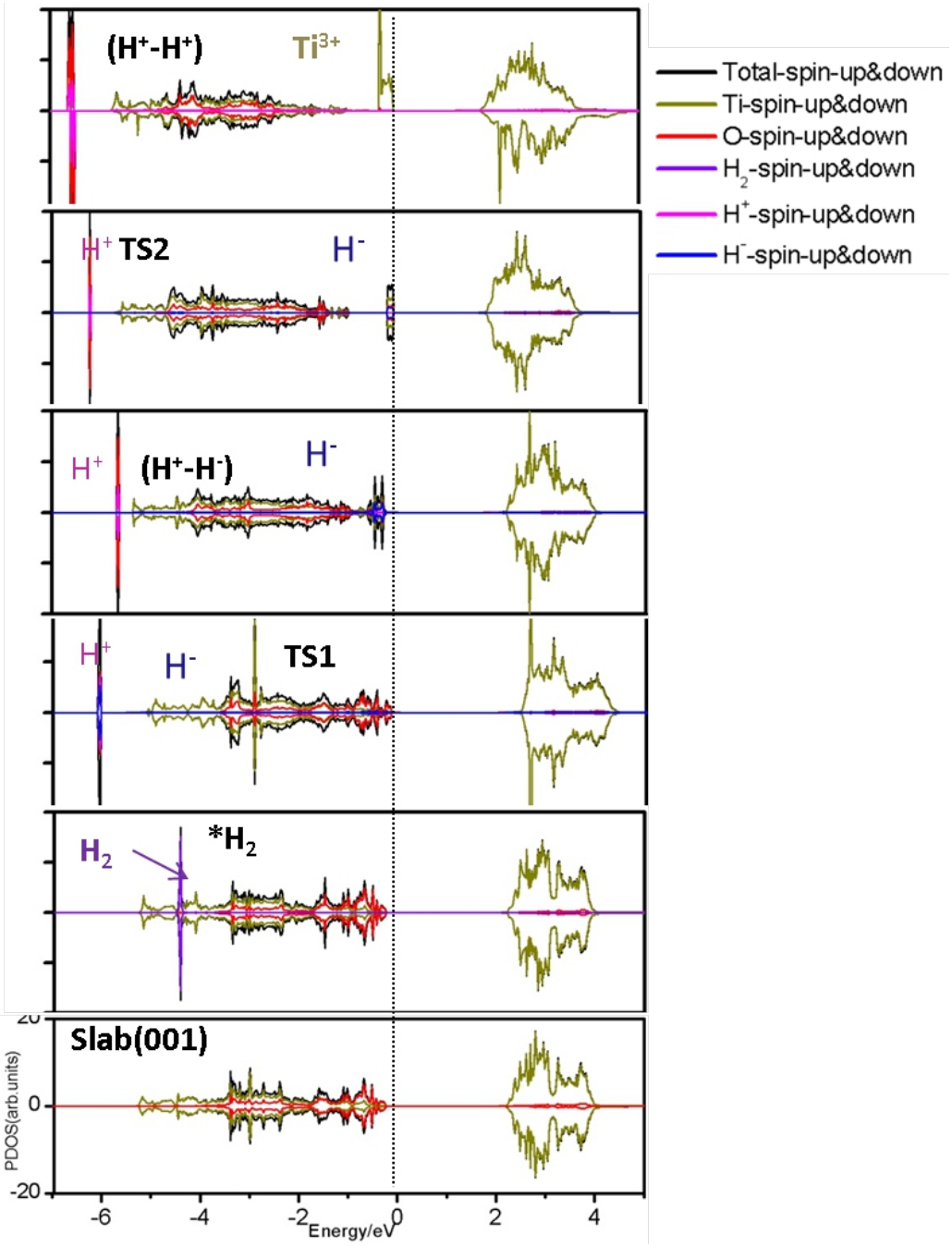

Figure 5: Total and projected density of states (PDOS) of the anatase TiO_2 slab, H_2, TS1, (H^+-H^-), and (H^+-H^+) for the (001) surfaces. For the PDOS, only the TiO and H involved in the two processes are projected. Positive density of states (DOS) correspond to spin up and negative to spin down.

existence of unpaired electrons. Two Ti ions are reduced, generating Ti^{3+} sites.

Bader charges analysis reported in Table 3 shows the electronic charges during the dissociation processes: first, the species H_2* was pre-activated with a slight polarization of H-H bond. For the TS species, the polarization of the H-H bond increases, forming an ion pair. And then, a hydride and proton were formed, which are identified with their Bader charges: (H^+-H) where the hydride species carries -0.3|e|. Besides, the oxygen involving the hydrogen transfer process generating hydroxyl group indicates an electron gain: approximately +0.3|e| compared to the same oxygen in the slab. The homolytic product containing two reduced titanium sites exhibits spin density in those sites, as shown in Figure 6. The integrated Bader spin shows the unpaired electrons for homolytic product (H^+-H+)are located in the Ti atoms (Figure 4.

The charge density difference of (H^+-H) compared to bare surface was investigated (Figure S10), indicating the electron gain and depletion during the heterolytic process.

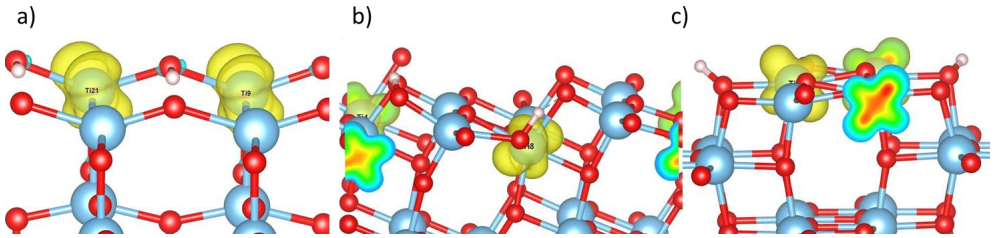

Figure 6: Spin density of (H^+-H^+) species, indicating the distribution of unpaired electrons on three anatase facets(001)(left), (100)(middle) and (100)(right)

3.3. IR Spectra

The infrared (IR) spectra were computed for all the (H^+-H^-) species on three anatase facets and are reported in Table 5 and Figure 7. The low-frequency modes of Ti–H and O–H are in the region of 500–900 cm^{-1}); O–H stretching modes show higher frequencies in the region of 1680–1700 cm^{-1} and 3570–3805 cm^{-1}. The frequencies of Ti-H stretching modes on three facets are very similar, around 1700 cm^{-1}, which correspond to the Ti-H IR spectral region (around 1600 cm^{-1}) found for rutile in our previous work[32, 51].

Table 3: Bader charge of involved H, Ti and O in the H_2 dissociation process.

slab	slab	H_2*	TS1	(H^+-H^-)	TS2	(H^+-H^+)
	q_{Ti}/q_O	qH/qH q_{Ti}/q_O				
(001)	2.00/-1.01	0.00/0.00	-0.29/0.31	-0.33/0.62	-0.22/0.63	0.65/0.62
		2.01/-1.01	2.00/-0.98	1.96/-0.97	1.93/-0.94	1.81/-1.27
(100)	1.98/-1.10	0.16/0.29	-0.32/0.37	-0.33/0.69	0.19/0.67	0.65/0.70
		1.96/-1.12	1.99/-1.10	1.94/-1.07	1.64/-1.07	1.84/-1.29
(101)	2.02/-1.05	0.42/0.34	-0.34/0.41	-0.31/0.63	0.04/0.73	0.74/0.65
		1.93/-1.07	2.00/-1.04	1.96/-1.04	1.81/-1.06	2.02/-1.31

Table 4: the integrated Bader spin for all the involved species in the process

	(001)		(100)		(110)	
species	TS2	(H^+-H^+)	TS2	(H^+-H^+)	TS2	(H^+-H^+)
Ti	0.97	0.98	0.98	0.99	0.98	0.98
Ti	0.93	0.99	0.94	0.99	0.96	0.99
O	0.00	0.00	0.00	0.00	0.00	0.00
O	0.03	0.00	0.00	0.00	0.00	0.00
H	0.00	0.00	0.00	0.00	0.00	0.00

Table 5: Wave-numbers (in cm^{-1}) and Their Relative Intensities (in brackets) of Ti-H^- and OH^+ Stretching Modes of (H^+-H^-) Species for three anatase facets.

	$\mu^{stretch}_{Ti-H}$	$\mu^{stretch}_{O-H}$
(001)	1685.2(0.06)	3578.8(0.03)
(100)	1685.3(0.91)	3770.6(0.20)
(101)	1700.4(0.34)	3804.1(0.17)

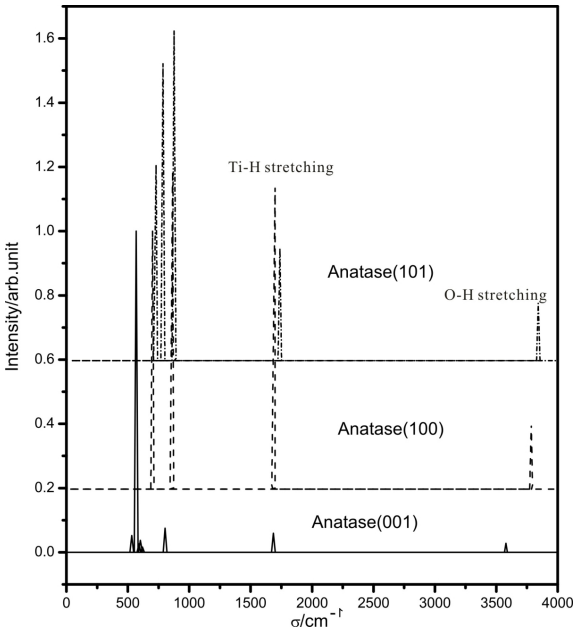

Figure 7: Computed IR spectra of the (H^+-H^-) species for Anatase (001),(100) and (101) surfaces

Experimentally, the OH stretching vibrations from water adsorption are observed at 3680 and 3610 cm^{-1}, most likely assigned to terminal hydroxyl groups[52], which is consistent with our values (3579-3804 cm^{-1}). TiH stretching modes of the species are seen in the calculated spectrum at 1685 cm^{-1} (001), 1685 cm^{-1} (100), and 1700 cm^{-1} (101), corresponding to the expected TiH IR spectral region (around 1600 cm^{-1})[53].

3.4. Descriptors of Reactivity

As regards the electronic structure, we found that the heterolytic activation barrier is linearly related to the Fermi energy difference between the heterolytic product (H^+-H^-) and the bare slab (Figure 8). The activation barriers are lower when the Fermi energy of hydride species (H^+-H^-) is closer to the one of the corresponding bare slab. This behavior was also found in the H_2 dissociation on ceria [29] as well as in metals with the hydrogen evolution reactions[54].

The relationship between structure and the reactivity is also studied. Interestingly, the analysis of the transition structures (TS1) indicates that several bond distances correlate with the barrier of the heterolytic dissociation

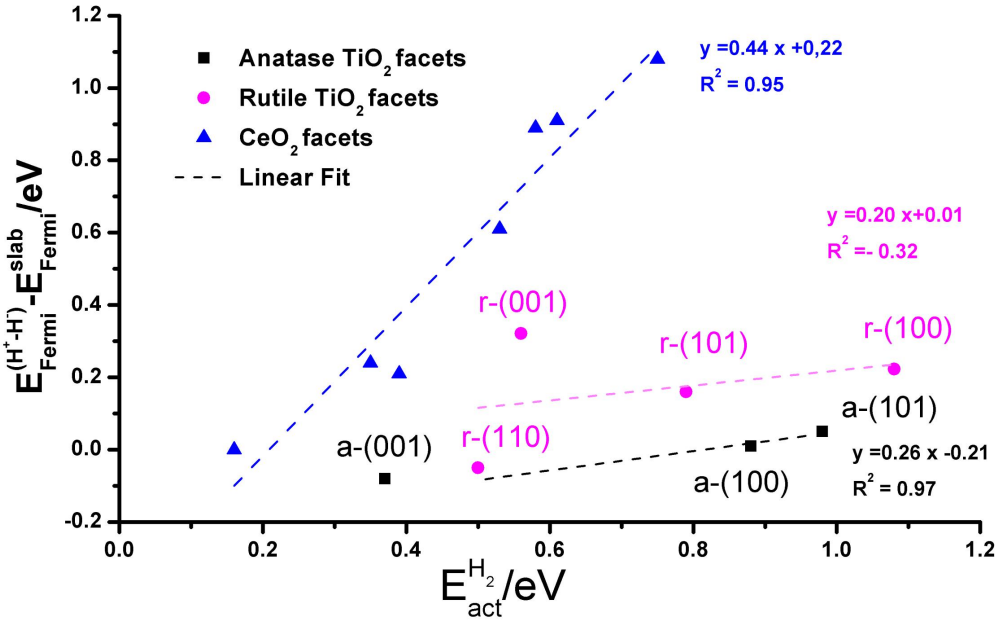

Figure 8: The heterolytic activation barrier as a function of the Fermi level difference between (H^+-H^-) and bare slab for different CeO_2 (blue point line), rutile (pink point line) and anatase TiO_2 facets (black point line).

of H_2. In TS1, the H_2 is polarized, pointing to a Ti and an O on the surface. The distances of Ti-H, H-H, and O-H in TS1 are between the adsorbed H_2* and hydride (H^+, H^-): on these three anatase facets, the distances of H-H span from 0.901 Å to 1.100 Å; Ti-H values span from 1.921 Å to 1.979 Å, and O-H distances span from 1.244 Å to 1.368 Å. More precisely, TS with lower energy barrier is associated to a structure close to the absorbed H_2* state (shorter H-H bonds and larger Ti-H and O-H distances) (see Table 6 and Figure 9). Such behavior is also found for ceria [29].

Table 6: Distance (Å) of H-H, Ti-H and O-H for Transition State Structure in heterolytic dissociation process.

	d(H-H)	d(Ti-H)	d(O-H)
(001)	1.719	1.746	0.982
(100)	1.062	1.907	1.201
(101)	1.095	1.878	1.174

The activation barrier as a function of the reaction energy of this heterolytic dissociation process is provided in SI (Table S2 and Figure S11 (black line)). It is indicated that, on these three anatase terminations, the thermodynamic reaction energies and the kinetic barriers follows a trend: the termination with the most exothermic reaction energy exhibits the highest reactivity. The termination with more endothermic reaction energy exhibits the poorest reactivity. The linear correlation is found on CeO_2 surfaces, see SI (Figure S10 (green line)), while it is not found for rutile phase.

Besides, in ceria, the shorter the Ce-O distance of bare slab, the smaller energy barrier [29], while no similar behavior was found for the anatase or rutile surfaces [32]. Two main factors can be at the origin of this effect. First, the topology of the surface plays a key role in stabilizing intermediates and TS. Second, the ionicity of the M-O bond in the substrate may help stabilizing polarized systems such as TS1 and (H^+-H^-). In the case of ceria, an ionic oxide, a clear linear correlation is observed whereas in titania, with more covalent character, orbital effects could be more important.

Moreover, to understand the trend of activation barriers of hydrogen transfer from Ti to O on the three terminations, we analysed the transition state (TS2) associated with this process. The higher barriers for (100) and (101) come from the long distance in space (over 3Å) of H transfer from Ti to nearby O (See Figure 10, middle and right). While the distance for H transfer from Ti to nearby 2-fold coordinated O on termination (001) is

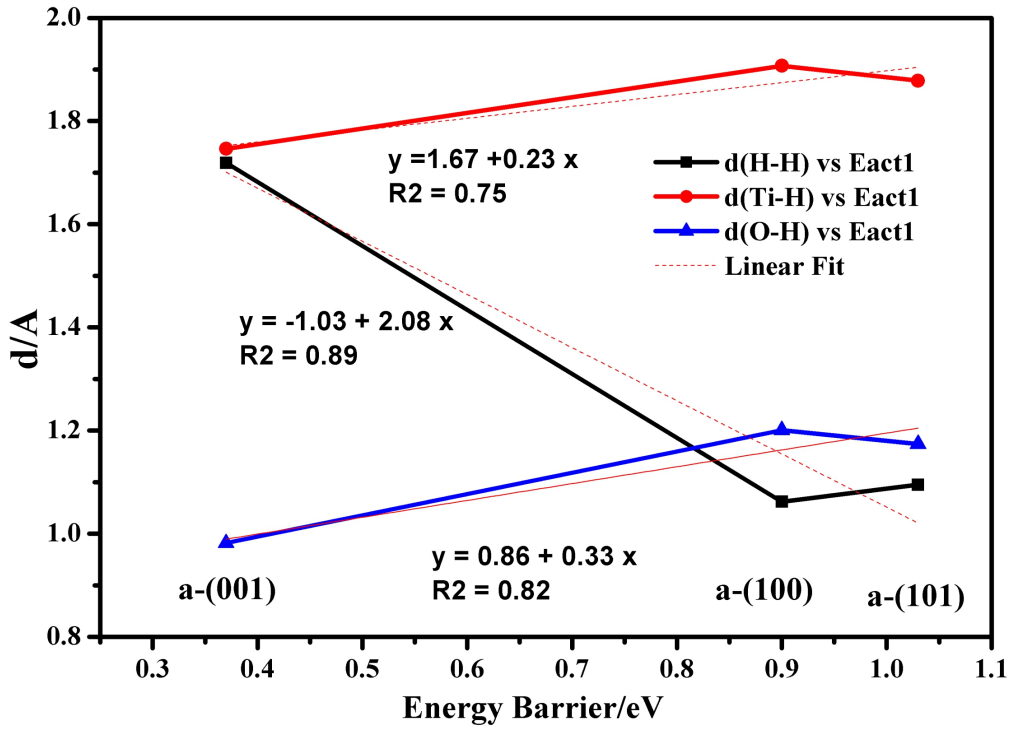

Figure 9: The distance of H-H, Ti-H and O-H bonds of TS1 as a function of heterolytic activation barrier for these three facets (001), (100) and (101), which are shown with red, black and blue line respectively.

much shorter, 2.471Å(see Figure 10, left), leading to a lower transfer barrier. We also check the reaction energy and H transfer barrier on three anatase facets (Table S2 and Figure S10 (black line)), no correlations between them were found. Neither for rutile surfaces.

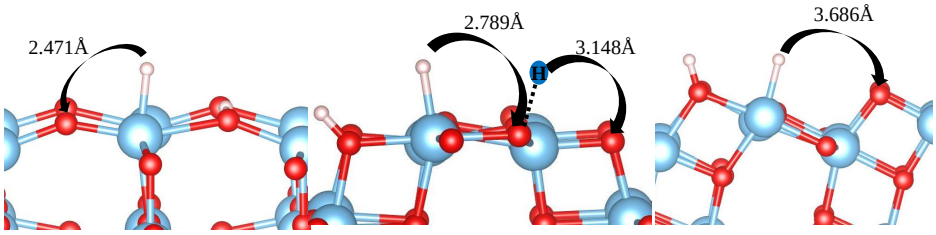

Figure 10: The distance of H transfer from Ti to O on (001) (left),(100) (middle) and (101) (right) facets.

4. Conclusion

A systematic study for adsorption and dissociation of H_2 on three anatase surfaces (001), (100), and (101) has been carried out employing DFT calculations. In summary, our study points out that dissociative H_2 adsorption on anatase TiO_2 takes place through a heterolytic pathway followed by the transfer of an H atom from a Ti atom to a nearby O atom that finally yields the homolytic product. The topology of the surface plays a crucial role in H_2 dissociation on titanium dioxide. On anatase (001), the two pathways are more favorable thermodynamically and kinetically than the other two surfaces. In addition, we have shown that Fermi energy can be used as the predictive descriptors of reactivity. Finally, the bond lengths of Ti-O, H-H and O-H in TS1 are associated with heterolytic dissociation activation barrier. The lower energy barrier is associated to a TS structure close to the absorbed H_2* state with shorter H-H bonds and larger Ti-H and O-H distances.

IR vibrational spectra of the homolytic product were also calculated indicating the expected vibrational region of hydride species on anatase TiO_2 surfaces is around 1700 cm^{-1}.

Some common features were found between titania and ceria, namely the heterolytic product and the hydride M-H species seems to play a role in the dissociation mechanism. Also, the homolytic product is thermodynamically stable. However, quantitative correlations between geometry (especially for

bare slab) and activation barriers were found to be apparent for ceria and not in titania. The nature of the M-O bond, mainly ionic in ceria and with a covalent characteri in titania, could be at the origin of the differences observed.

5. Supporting information

Supporting information can be found in the online version.

6. CRediT authorship contribution statement

Baohuan Wei: Investigation, writing—original draft, and editing; Monica Calatayud: software, supervision, writing—review and editing,

7. Declaration of Competing Interest

The authors declare that they have no known competing financial interests or personal relationships that could have appeared to influence the work reported in this paper.

8. acknowledgement

This study was supported by China Scholarship Council (CSC). Authors acknowledge Scienomics for the MAPS program used in the construction of the slab models for a courtesy license. Dr. B. Diawara is warmly acknowledged for the Modelview program. This work was performed using HPC resources from GENCI- CINES/IDRIS (Grant 2020- x2020082131),

9. Appendix A. Supplementary data

Supplementary material related to this article can be found, in the online version, at https://www.overleaf.com/read/vvjxrfftyvjf

10. References

References

[1] F. Amano, T. Yasumoto, O.-O. Prieto-Mahaney, S. Uchida, T. Shibayama, B. Ohtani, Photocatalytic activity of octahedral single-crystalline mesoparticles of anatase titanium (iv) oxide, Chemical communications (2009) 2311–2313.

[2] H. Tada, M. Fujishima, H. Kobayashi, Photodeposition of metal sulfide quantum dots on titanium (iv) dioxide and the applications to solar energy conversion, Chemical Society Reviews 40 (2011) 4232–4243.

[3] S. Iijima, Helical microtubules of graphitic carbon, nature 354 (1991) 56–58.

[4] D. Li, R. You, M. Yang, Y. Liu, K. Qian, S. Chen, T. Cao, Z. Zhang, J. Tian, W. Huang, Morphology-dependent evolutions of sizes, structures, and catalytic activity of au nanoparticles on anatase tio_2 nanocrystals, The Journal of Physical Chemistry C 123 (2019) 10367–10376.

[5] D. I. Enache, J. K. Edwards, P. Landon, B. Solsona-Espriu, A. F. Carley, A. A. Herzing, M. Watanabe, C. J. Kiely, D. W. Knight, G. J. Hutchings, Solvent-free oxidation of primary alcohols to aldehydes using au-pd/tio_2 catalysts, Science 311 (2006) 362–365.

[6] X. Zhou, Z. Wang, X. Xia, G. Shao, K. Homewood, Y. Gao, Synergistic cooperation of rutile tio_2 {002},{101}, and {110} facets for hydrogen sensing, ACS applied materials & interfaces 10 (2018) 28199–28209.

[7] W. Zhou, G. Du, P. Hu, G. Li, D. Wang, H. Liu, J. Wang, R. I. Boughton, D. Liu, H. Jiang, Nanoheterostructures on tio_2 nanobelts achieved by acid hydrothermal method with enhanced photocatalytic and gas sensitive performance, Journal of Materials Chemistry 21 (2011) 7937–7945.

[8] P. G. Bruce, B. Scrosati, J.-M. Tarascon, Nanomaterials for rechargeable lithium batteries, Angewandte Chemie International Edition 47 (2008) 2930–2946.

[9] Y.-G. Kim, J. Walker, L. A. Samuelson, J. Kumar, Efficient light harvesting polymers for nanocrystalline tio_2 photovoltaic cells, Nano Letters 3 (2003) 523–525.

[10] L. H. Slooff, J. M. Kroon, J. Loos, M. M. Koetse, J. Sweelssen, Influence of the relative humidity on the performance of polymer/tio_2 photovoltaic cells, Advanced Functional Materials 15 (2005) 689–694.

[11] M. Ranade, A. Navrotsky, H. Zhang, J. Banfield, S. Elder, A. Zaban, P. Borse, S. Kulkarni, G. Doran, H. Whitfield, Energetics of nanocrystalline tio_2, Proceedings of the National Academy of Sciences 99 (2002) 6476–6481.

[12] A. Cuko, M. Calatayud, S. T. Bromley, Stability of mixed-oxide titanosilicates: dependency on size and composition from nanocluster to bulk, Nanoscale 10 (2018) 832–842.

[13] M. Setvin, M. Buchholz, W. Hou, C. Zhang, B. Stoger, J. Hulva, T. Simschitz, X. Shi, J. Pavelec, G. S. Parkinson, et al., A multitechnique study of co adsorption on the tio_2 anatase (101) surface, The Journal of Physical Chemistry C 119 (2015) 21044–21052.

[14] U. Aschauer, A. Selloni, Hydrogen interaction with the anatase tio_2 (101) surface, Physical Chemistry Chemical Physics 14 (2012) 16595–16602.

[15] M. Setvin, J. Hulva, H. Wang, T. Simschitz, M. Schmid, G. S. Parkinson, C. Di Valentin, A. Selloni, U. Diebold, Formaldehyde adsorption on the anatase tio_2 (101) surface: experimental and theoretical investigation, The Journal of Physical Chemistry C 121 (2017) 8914–8922.

[16] M. Setvin, X. Shi, J. Hulva, T. Simschitz, G. S. Parkinson, M. Schmid, C. Di Valentin, A. Selloni, U. Diebold, Methanol on anatase tio_2 (101): Mechanistic insights into photocatalysis, ACS catalysis 7 (2017) 7081–7091.

[17] E. German, R. Faccio, Á. W. Mombrú, Theoretical study of new potential semiconductor surfaces performance for dye sensitized solar cell usage: Tio_2-b (001),(100) and $h_2ti_3o_7$ (100), Applied Surface Science 426 (2017) 1182–1189.

[18] H. Kusama, H. Orita, H. Sugihara, Tio_2 band shift by nitrogen-containing heterocycles in dye-sensitized solar cells: a periodic density functional theory study, Langmuir 24 (2008) 4411–4419.

[19] G. Martra, Lewis acid and base sites at the surface of microcrystalline tio_2 anatase: relationships between surface morphology and chemical behaviour, Applied Catalysis A: General 200 (2000) 275–285.

[20] M. Calatayud, C. Minot, Effect of relaxation on structure and reactivity of anatase (1 0 0) and (0 0 1) surfaces, Surface science 552 (2004) 169–179.

[21] S. Liu, J. Yu, M. Jaroniec, Anatase tio_2 with dominant high-energy {001} facets: synthesis, properties, and applications, Chemistry of Materials 23 (2011) 4085–4093.

[22] N. Roy, Y. Sohn, D. Pradhan, Synergy of low-energy {101} and high-energy {001} tio_2 crystal facets for enhanced photocatalysis, ACS nano 7 (2013) 2532–2540.

[23] X.-Q. Gong, A. Selloni, Reactivity of anatase tio_2 nanoparticles: the role of the minority (001) surface, The Journal of Physical Chemistry B 109 (2005) 19560–19562.

[24] A. Hussain, J. Gracia, B. E. Nieuwenhuys, J. Niemantsverdriet, Chemistry of o-and h-containing species on the (001) surface of anatase tio_2: a dft study, ChemPhysChem 11 (2010) 2375–2382.

[25] U. Diebold, The surface science of titanium dioxide, Surface science reports 48 (2003) 53–229.

[26] X.-L. Yin, M. Calatayud, H. Qiu, Y. Wang, A. Birkner, C. Minot, C. Wöll, Diffusion versus desorption: complex behavior of h atoms on an oxide surface, ChemPhysChem 9 (2008) 253–256.

[27] H.-R. An, Y. C. Hong, H. Kim, J. Y. Huh, E. C. Park, S. Y. Park, Y. Jeong, J.-I. Park, J.-P. Kim, Y.-C. Lee, et al., Studies on mass production and highly solar light photocatalytic properties of gray hydrogenated-tio_2 sphere photocatalysts, Journal of hazardous materials 358 (2018) 222–233.

[28] M. Lei, S. Coh, Hydrogen plasma favored modification of anatase TiO_2 (001) surface with desirable water splitting performance, Phys. Rev. Materials 4 (2020) 075801. URL: https://link.aps.org/doi/10.1103/PhysRevMaterials.4.075801. doi:10.1103/PhysRevMaterials.4.075801.

[29] O. Matz, M. Calatayud, Breaking h_2 with ceo_2: Effect of surface termination, ACS omega 3 (2018) 16063–16073.

[30] M. V. Ganduglia-Pirovano, C. Popa, J. Sauer, H. Abbott, A. Uhl, M. Baron, D. Stacchiola, O. Bondarchuk, S. Shaikhutdinov, H.-J. Freund, Role of ceria in oxidative dehydrogenation on supported vanadia catalysts, Journal of the American Chemical Society 132 (2010) 2345–2349.

[31] M. Garcia-Melchor, N. Lopez, Homolytic products from heterolytic paths in h_2 dissociation on metal oxides: the example of ceo_2, The Journal of Physical Chemistry C 118 (2014) 10921–10926.

[32] B. Wei, F. Tielens, M. Calatayud, Understanding the role of rutile tio_2 surface orientation on molecular hydrogen activation, Nanomaterials 9 (2019) 1199.

[33] G. Hu, Z. Wu, D.-e. Jiang, First principles insight into h_2 activation and hydride species on tio_2 surfaces, The Journal of Physical Chemistry C 122 (2018) 20323–20328.

[34] M. M. Islam, M. Calatayud, G. Pacchioni, Hydrogen adsorption and diffusion on the anatase tio_2 (101) surface: a first-principles investigation, The Journal of Physical Chemistry C 115 (2011) 6809–6814.

[35] C. Sun, Y. Jia, X.-H. Yang, H.-G. Yang, X. Yao, G. Q. Lu, A. Selloni, S. C. Smith, Hydrogen incorporation and storage in well-defined nanocrystals of anatase titanium dioxide, The Journal of Physical Chemistry C 115 (2011) 25590–25594.

[36] O. A. Syzgantseva, P. Gonzalez-Navarrete, M. Calatayud, S. Bromley, C. Minot, Theoretical investigation of the hydrogenation of (tio_2) n clusters (n= 1–10), The Journal of Physical Chemistry C 115 (2011) 15890–15899.

[37] Y. Yan, W. Shi, Z. Yuan, S. He, D. Li, Q. Meng, H. Ji, C. Chen, W. Ma, J. Zhao, The formation of ti–h species at interface is lethal to the efficiency of tio_2-based dye-sensitized devices, Journal of the American Chemical Society 139 (2017) 2083–2089.

[38] M. Calatayud, C. Minot, Is there a nanosize for the activity of tio_2 compounds?, The Journal of Physical Chemistry C 113 (2009) 12186–12194.

[39] G. Kresse, J. non-cryst. solid, 1995, 193, 222-229;(b) g. kresse and j. hafner, Phys. Rev. B 49 (1994) 14251–14264.

[40] P. E. Blöchl, Projector augmented-wave method, Physical review B 50 (1994) 17953.

[41] J. P. Perdew, K. Burke, M. Ernzerhof, Generalized gradient approximation made simple, Physical review letters 77 (1996) 3865.

[42] S. Dudarev, G. Botton, S. Savrasov, C. Humphreys, A. Sutton, Electron-energy-loss spectra and the structural stability of nickel oxide: An lsda+ u study, Physical Review B 57 (1998) 1505.

[43] S. Ma, S.-D. Huang, Y.-H. Fang, Z.-P. Liu, Tih hydride formed on amorphous black titania: Unprecedented active species for photocatalytic hydrogen evolution, ACS Catalysis 8 (2018) 9711–9721.

[44] G. Henkelman, H. Jónsson, Improved tangent estimate in the nudged elastic band method for finding minimum energy paths and saddle points, The Journal of chemical physics 113 (2000) 9978–9985.

[45] G. Henkelman, B. P. Uberuaga, H. Jónsson, A climbing image nudged elastic band method for finding saddle points and minimum energy paths, The Journal of chemical physics 113 (2000) 9901–9904.

[46] A. Heyden, A. T. Bell, F. J. Keil, Efficient methods for finding transition states in chemical reactions: Comparison of improved dimer method and partitioned rational function optimization method, The Journal of chemical physics 123 (2005) 224101.

[47] G. Henkelman, H. Jónsson, A dimer method for finding saddle points on high dimensional potential surfaces using only first derivatives, The Journal of chemical physics 111 (1999) 7010–7022.

[48] G. Kyriakou, E. R. Davidson, G. Peng, L. T. Roling, S. Singh, M. B. Boucher, M. D. Marcinkowski, M. Mavrikakis, A. Michaelides, E. C. H. Sykes, Significant quantum effects in hydrogen activation, ACS nano 8 (2014) 4827–4835.

[49] S. Baroni, S. De Gironcoli, A. Dal Corso, P. Giannozzi, Phonons and related crystal properties from density-functional perturbation theory, Reviews of modern Physics 73 (2001) 515.

[50] J. K. Burdett, T. Hughbanks, G. J. Miller, J. W. Richardson Jr, J. V. Smith, Structural-electronic relationships in inorganic solids: powder neutron diffraction studies of the rutile and anatase polymorphs of titanium dioxide at 15 and 295 k, Journal of the American Chemical Society 109 (1987) 3639–3646.

[51] A. Mahdavi-Shakib, J. M. Arce-Ramos, R. N. Austin, T. J. Schwartz, L. C. Grabow, B. G. Frederick, Frequencies and thermal stability of isolated surface hydroxyls on pyrogenic tio_2 nanoparticles, The Journal of Physical Chemistry C 123 (2019) 24533–24548.

[52] P. Jones, J. Hockey, Infra-red studies of rutile surfaces. part 2.-hydroxylation, hydration and structure of rutile surfaces, Transactions of the Faraday Society 67 (1971) 2679–2685.

[53] C. Coperet, D. P. Estes, K. Larmier, K. Searles, Isolated surface hydrides: Formation, structure, and reactivity, Chemical reviews 116 (2016) 8463–8505.

[54] E. Santos, P. Quaino, W. Schmickler, Theory of electrocatalysis: hydrogen evolution and more, Physical Chemistry Chemical Physics 14 (2012) 11224–11233.